
Introduction of the seepage device for examining the one to four hundred model of the Karkheh Dam.

Ali Mahbod^{1*}, Hamid Reza Saba², Mostafa Yousofi Rad³, Hamid Lajvardi⁴

1. Civil Engineering Group, Arak Branch, Islamic Azad University, Arak, Iran

2. Assistant Professor, Faculty of Civil Engineering, Tafresh University, Iran

3. Geology Group, Faculty of Earth Sciences, Arak Industrial University, Iran

4. Civil Engineering Group, Arak Branch, Islamic Azad University, Arak, Iran

ARTICLE INFO

Keywords:

Cutoff Wall, Earth Dam, Plaxis, Seepage Test

ABSTRACT

Earth dams, as one of the largest earthen structures, are subjected to various failure mechanisms, some of which, such as cracking and hydraulic failure, occur within the dam body, while other mechanisms like liquefaction, divergence, and dissolution arise from the geotechnical properties of the foundation or the region's bed. In this research, which is derived from a doctoral dissertation, an evaluation of the geomechanical parameters affecting the occurrence of hydraulic failure was conducted to understand the interaction between the dam body and these parameters and to provide a safe model for reducing the risk of constructing earth dams and studying ways to address problematic foundations. The modeling of the issue was performed using the finite element numerical method with the PLAXIS computational code. In this laboratory study, by varying the mixing percentage of the materials in the cutoff wall, their effects on the behavior of the earth dam were investigated. The results indicated that the laboratory results presented in this research have a suitable overlap with the software results, and using this device, the seepage in each mixing design can be calculated based on dimensional analysis.

Introduction

Usually, excessive seepage must be prevented behind earth dams. The use of plastic concrete cutoff walls reduces seepage through the dam. Additionally, the cutoff wall, as a component of the earth dam, must not only maintain stability but also possess adequate flexibility.

In this study, a heterogeneous earth dam was numerically investigated. This dam is situated on a foundation with heterogeneous layers. Various modeling was conducted using Plaxis software. The effects of different parameters on the dynamic behavior of the dam were examined.

Based on the obtained values, a combination of one cubic meter of concrete with internal friction angle of 18 degrees, cohesion of 1500 kPa, and Young's modulus of 1500 MPa is recommended; these values were derived based on the maximum displacement of the cutoff wall without failure occurring and considering the parametric changes made to the input parameters.

For the construction of cutoff walls using plastic concrete or structural concrete, a panel method is employed. One consequence of this method is that due to the erosion of the materials, the acceptable performance of the wall as a seepage control measure is called into question [Rahimi, 1389].

Vertical soil-bentonite cutoff walls installed using the trenching technology have widespread applications in the United States, Canada, and Japan for controlling subsurface contamination displacement [Hu et al, 2010].

The impact of the amount of fines, the amount of bentonite, the grading of sand, and the type and amount of additives (such as zeolite and activated carbon) on permeability and hydraulic conductivity (k) has been extensively studied, as they relate to the relationships between permeability and the lateral resistance of sandy/bentonite earth embankments (SB) and sand/clay (SC) [Du et al, 2014]. The soil-bentonite embankment typically has an undrained shear strength that, due to its relatively high moisture content, is less than 10 kPa, and in the presence of external loads, strength is one of the main design parameters [Xue et al, 2013]. Studies indicate that compared to Na-bentonite embankments, old sandy soils, SB clay embankments with moisture content between 5 to 15 percent perform well in terms of compressibility and hydraulic conductivity [Evans et al, 1995]. A significant increase (for example, 4 to 10 times) in hydraulic conductivity may also occur, which, upon contact with chemical liquids, may lead to failure, provided that the specific monitoring of sandy SB and Na-bentonite embankments is adhered to. Changes in the engineering properties of engineered soil barriers can be attributed to the following: (1) shrinkage of the double layer dispersing bentonite particles due to increased concentrations of pore water metals, (2) degradation of carbon bonds or cementation between clay particles due to acid corrosion, and (3) complex geochemical and mineralogical changes [Shama & Shackelford, 2004].

Previous studies have shown that initial moisture content can significantly affect clean and contaminated SB clay embankments as well as disturbed natural clay [Malusis et al, 2010].

With an increase in the average effective vertical consolidation stress, the consolidation coefficient slightly increases, which is consistent with old Na-bentonite/sandy soil embankments. This is primarily controlled by the rate of excess pore pressure dissipation. Furthermore, the increase in c_v , with the increase in average effective vertical stress, results from a larger change in m_v compared to hydraulic conductivity [Ruffing et al, 2010]. Such observations have also been reported in previous studies for Na-bentonite/sandy soil embankments, Na-bentonite/activated carbon modified sandy embankments, and Na-bentonite/zeolite modified sandy embankments. Fields (1996) and Ruffing et al. (2010) suggested that the lateral earth pressure effective on soil-bentonite embankments can be much lower than the geostatic pressure, estimated to be less than 100kPa based on the modified lateral pressure model [Hong et al, 2010]. There is a threshold concentration beyond which the effect of pb or Ca concentration on changes in hydraulic conductivity is negligible. The threshold amount of pb or Ca concentration for the embankment

presented here and the sandy SB embankment reported by Malusis and McKeon (2013) varies from 500 to 130 mmol/l depending on the amount of bentonite. The range of hydraulic conductivity ratios for sandy SB embankments reported by Malusis and McKeon (2013) varies from 3.5 to 16. Possible reasons for this discrepancy include: (1) the hydraulic conductivity of the embankments in this study was calculated based on one-dimensional Terzaghi consolidation theory, (2) the SB clay embankments tested here were prepared by mixing a clay (kaolin)-Ca-bentonite mixture with Pb(NO₃) solution, and (3) in this study, Ca-bentonite was used, while Malusis and McKeon used Na-bentonite [Fan et al., 2014].

According to the Ball-Chapman theory (Michel and Soga, 2005), with the increase in Pb concentration, the degree of contraction of the double layer of the dispersant or the reduction of the swelling potential of bentonite will increase, which leads to a decrease in the liquid limit and an increase in the hydraulic conductivity of bentonite, as suggested by Esridhaharan et al. (2007) and Horpi Bulski et al. (2011) [Malusis & McKeehan, 2013].

The modeling of the problem was performed using the finite element numerical method with the PLAXIS computational code. In this numerical study, the effects of important parameters including internal friction angle, cohesion, and Young's modulus on the dynamic behavior of the dam were examined. During this process, by disregarding cases that failed in the modeling, the stability of the dam was ensured in all conditions and results. The outputs of Plaxis included total displacement in the cutoff wall, mesh changes, changes in pore water pressure throughout the dam body and in the cutoff wall, to consider the overall effects of all influencing factors on the flexibility conditions of the dam's cutoff wall. To validate the numerical modeling, the obtained results were compared with the actual values taken from the Karkheh Dam, and then to achieve suitable conditions including maximum flexibility, minimum pore water pressure, and the finest meshing, the results were presented as the required percentage change in materials. The flexibility of the cutoff wall was considered as the maximum displacement of the cutoff wall without any failure occurring in it, and an optimal combination of materials for one cubic meter of concrete was proposed.

Due to the time-consuming nature of numerical modeling for model development, a program was designed in Matlab that calculates each of the output values based on the input values. Then, for each of the outputs, an active graph is drawn. The error percentage of the program is at an acceptable level.

Introduction to the studied dam:

The Karkheh earth dam has a clay core, a maximum base width of 1100 meters, a crest width of 12 meters, a crest length of 3030 meters, a crest height from the base of 127 meters, and a total reservoir volume of 3.7 billion cubic meters [Yong et al., 2009]. Its site consists of heterogeneous layers of Bakhtiari conglomerate, with mechanical properties of the layers not being uniform in different directions, and its calcareous cementation is also incomplete, having relatively high permeability with sandy open channels. Between the layers of gravel and sand lenses with very low permeability are located among the conglomerate layers. The Karkheh conglomerate contains 45% chert and silica and has high abrasiveness. One of the important features of the Karkheh conglomerate is its high permeability and low injectability to control seepage from the dam's base. Due to this characteristic of the conglomerate, after conducting an injection test during the studies and failing to create a continuous cutoff curtain and achieving negligible permeability reduction after injection, the option of a cutoff wall was chosen and designed instead. The cutoff wall of the Karkheh Dam is 2940 meters long, with a variable depth of 18 to 78 meters and thicknesses of 80 and 100 centimeters, covering a total area of 162,000 m², made of plastic concrete and constructed

using the wet method. The axis of the cutoff wall is aligned with the dam and is created in the middle of the clay core [31]. In the middle sections of the dam, the cutoff wall is connected to one of the gravel layers, and in the side sections, parts of the wall are suspended in the conglomerate layer.

Numerical modeling:

Considering the use of the Plaxis computational code, in this research work, to ensure the accuracy of the outputs and the validation of the method used, an earth dam whose dynamic analysis results are available in a reliable source was modeled, and the accuracy of the results was examined. To further ensure the outputs and eliminate any potential errors, the Karkheh earth dam was selected, which had previously been analyzed by Tabree and Abreshami (1397).

Given that the maximum height of the Karkheh dam is 127 meters, the maximum stress and pressure applied to the cutoff wall occurs at this section. Additionally, the conditions of the cutoff wall in this section pass through different layers of conglomerate and gravel, and there are layer-by-layer conditions around it, making this section the basis for static and dynamic analyses. In the studied section, 8 meters of the cutoff wall is embedded in the clay core, and after passing through the layers of conglomerate 1-, gravel 1-, and conglomerate 2-, it is embedded 2.5 meters within the gravel layer 2-. At the contact point of the clay core with the conglomerate base, a reinforcement trench made of plastic concrete with a maximum width of 14 meters and a minimum width of 8 meters and a thickness of 1.5 meters has been executed. For simulation, the largest cross-section of the dam was modeled as a plane strain using 15-node triangular elements, and the intersection of the cutoff wall and the base was simulated using joint elements. The first reservoir filling of the dam was selected as the critical static loading, and a static stress-strain analysis was performed.

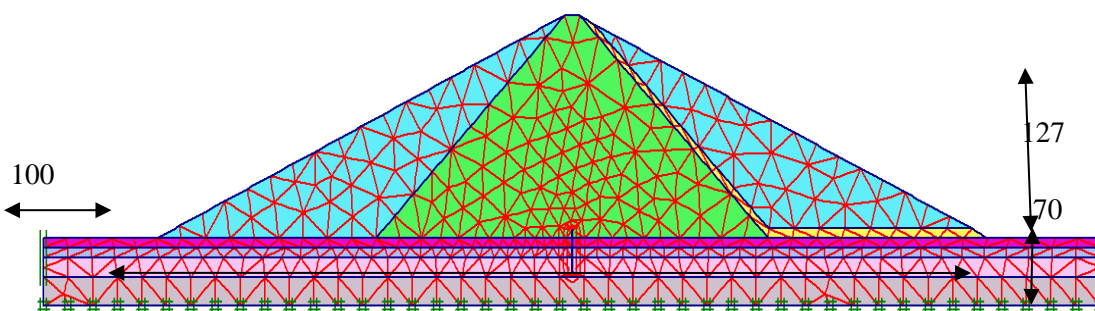
To simulate the problem, an earth dam with a clay core with a crest width of 10 meters and a height of 100 meters was modeled. For the downstream side of the dam, a zero elevation head was considered, aligned with the ground level downstream of the dam body. The upstream head of the dam was calculated based on the freeboard calculated at the base and the height of the dam crest (Formula 1). Due to the lack of necessary information regarding wind speed, according to USBR regulations, a wind speed of 160 kilometers per hour was considered. The fetch length was also assumed to be 20 kilometers, and the average reservoir depth was assumed to be 25 meters. Additionally, the upstream body wall of the dam was considered as riprap, which increases the wave effect by 1.5 times. A schematic of the external specifications of the modeled dam is presented in Figure 1.

$$Free\ Board = 1.5 \times \left(0.032\sqrt{F \cdot V} + 0.76F^{0.25} + \frac{V^2 F \cdot \cos A}{63000D} \right)$$

$$Free\ Board = 1.5 \times \left(0.032\sqrt{20 \cdot 160} + 0.76 \times 20^{0.25} + \frac{160^2 \times 20}{63000 \times 25} \right) = 3.5m$$

$$Free\ Board \approx 4m$$

$$Up\ stream\ Head = 98.5 - 4 = 94.5\ m$$



Figure

The specifications of the materials used in the modeling for a stone foundation with a thickness of 60 meters and with specific characteristics of unit weight 40 kPa, cohesion 100 kPa, and internal friction angle of 75 degrees are presented in Table 1. The geotechnical specifications of the materials used in the modeling are also provided in Table 1.

Table 1 - Geotechnical properties of materials used in modeling

Soil type	E (kN/m ²)	C (kN/m ²)	φ	K (m/day)
shell	5500	30	35	0.2
the core	2500	60	30	.001
foundation soil	3500	1	33	0.4
drain	30,000	1	35	10
Cut off wall	4000	1	33	0.05

In order to provide a comprehensive analysis of the water barrier wall, the parameters of the materials and the specifications of the water barrier wall must be evaluated within a reasonable range. Therefore, the maximum range of variations in the specifications of the water barrier wall materials has been determined and presented in Table 2.

Table 2 - Range of changes in the specifications of waterproofing wall materials

Soil type	Special Weight (kN/m ²)	φ	Relative density (percentage)	SPT
Sand loose	16.6<G<18.1	29< φ<33	Dr<35	4<N<10
Sand medium	18.1<G<19.3	33< φ <38	35 <Dr<65	10<N<30
Sand dense	19.3<G<20.4	38< φ <40	65 <Dr<85	30<N<50
Soil type	Special Weight (kN/m ²)	Adhesion (kN/m ²)	e50	SPT
clay soft	15.1<G<17.8	4< C<21	1.65<e<4.38	1<N<4
clay medium	17.8<G<20.2	21< C <57	0.9<e<1.65	4<N<10
clay stiff	20.2<G<20.8	57< C <94	0.66<e<0.9	10<N<16
clay very stiff	20.8<G<21.5	94< C <194	0.43<e<0.66	16<N<32
Soil type	Special Weight (kN/m ²)	Adhesion (kN/m ²)	φ	SPT
silt medium	17.9<G<20.2	10.4< C<29	27< φ<30	4<N<10
silt stiff	2.0.2<G<20.8	29< C <47	30< φ <32	10<N<16
silt very stiff	2.8<G<21.5	47< C <96	32< φ <35	16<N<32

The displacement diagram of the dam's water barrier in numerical modeling and the Tabrizi and Abrishami studies (2017) is presented in Figure 2. A comparison of the results shows that the results obtained from the validation have a similar trend, albeit with slight differences compared to the Tabrizi model.

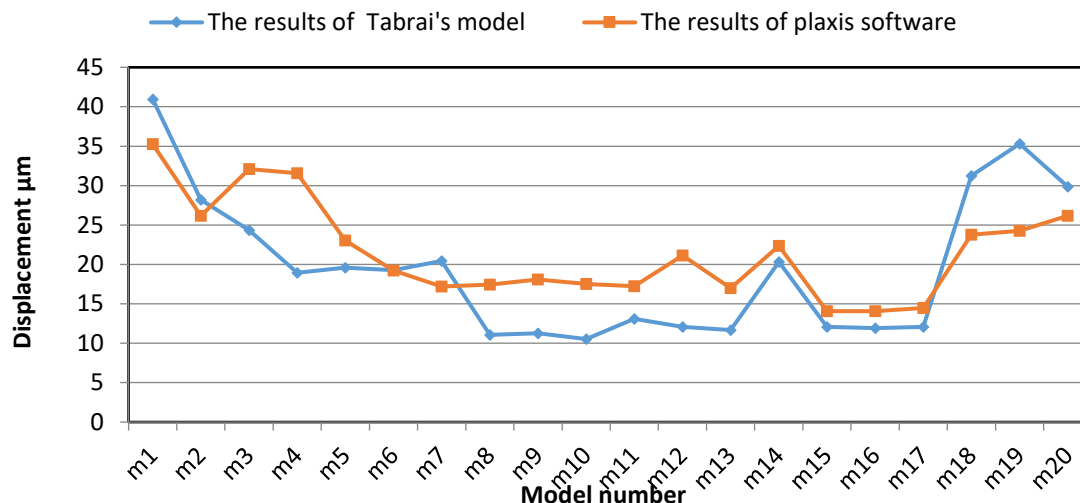


Figure 2 - Displacement diagram of the dam's water barrier in numerical modeling and Tabrizi (1397) and Abreshimi studies

Modeling and Analysis Process

The analyses began with an initial review and identification of critical points. In the initial review, three parameters—internal friction angle, cohesion, and Young's modulus—were each varied separately while keeping the other parameters constant within a specified range. To conduct a detailed examination and select critical points, the range for the internal friction angle was set from 0 to 50 degrees, cohesion from 1 kPa to 2000 kPa, and elastic modulus from 100 MPa to 2000 MPa. In the Plaxis software, a medium mesh was used, and to enhance accuracy, a finer mesh was applied around the impermeable wall. The best flexibility of the impermeable wall was considered as the maximum deformation in the wall without causing failure. Therefore, models that exhibited failure were excluded from the analyses. Additionally, to ensure greater reliability, the maximum change in the form of the elements throughout the dam body was also examined .

-1-1 Modeling with Plaxis :

The final models were developed based on the specifications and assumptions made in the initial review, focusing solely on the rotational change in the three parameters under consideration. Pore water pressure has an inverse effect on effective stress; thus, examining this factor is also essential. Consequently, this factor will be analyzed in the dam body and the impermeable wall ..

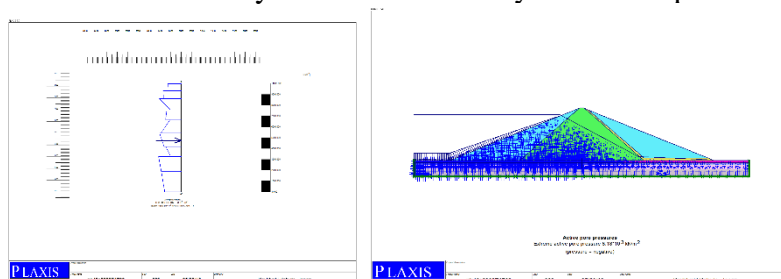


Figure 3: Examination of Pore Water Pressure

The above shapes indicate the position and conditions such as the pore water pressure, the position of the water surface, and the phreatic line throughout the dam. Additionally, the pore water pressure profile in the impermeable wall is provided under conditions of varying Poisson's ratio,

internal friction angle, and cohesion while keeping other conditions constant, which will be analyzed further.

Final Analysis Summary

Based on the analysis conducted by Plaxis, which was thoroughly examined in the previous section, the results can be reviewed as follows .

Table 3: Results of the Final Model

sample number	pore pressures (Cut off)	pore pressures (Dam)	Concrete specifications			sample number	pore pressures (Cut off)	pore pressures (Dam)	Concrete specifications		
			Phi	C	E				Phi	C	E
64	2.31	7.3	22	1500	1500	1	2.64	4.38	0	1300	100
65	2.57	7.87	22	1500	1700	2	2.47	5.47	0	1300	800
66	3.03	5.09	22	1900	100	3	2.51	5.67	0	1300	1300
67	4.36	5.17	22	1900	800	4	2.83	6.05	0	1300	1500
68	3.41	6.98	22	1900	1300	5	2.48	3.13	0	1300	1700
69	3.78	7.61	22	1900	1500	6	2.65	4.73	0	1400	100
70	4.05	8.19	22	1900	1700	7	2.75	5.56	0	1400	800
71	2.74	5.13	22	2000	100	8	3.29	5.89	0	1400	1300
72	3.14	5.17	22	2000	800	9	2.8	6.01	0	1400	1500
73	2.82	6.98	22	2000	1300	10	2.88	6.2	0	1500	1700
74	3.48	7.59	22	2000	1500	11	3.08	4.93	0	1500	100
75	2.39	8.22	22	2000	1700	12	3.2	5.88	0	1500	800
76	2.9	5.09	24	1300	100	13	2.96	6.04	0	1500	1300
77	2.71	5.2	24	1300	800	14	3.27	6.27	0	1500	1500
78	2.82	6.8	24	1300	1300	15	4.22	6.38	0	1500	1700
79	2.34	7.23	24	1300	1500	16	3.03	5.13	0	1900	100
80	2.77	7.53	24	1300	1700	17	3.03	5.15	0	1900	800
81	3.06	5.09	24	1400	100	18	3.37	6.75	0	1900	1300
82	4.82	5.19	24	1400	800	19	2.78	7.08	0	1900	1500
83	2.35	6.89	24	1400	1300	20	2.38	7.35	0	1900	1700

84	2.79	7.37	24	1400	1500	21	3.06	5.13	0	2000	100
85	3.01	7.75	24	1500	1700	22	2.49	5.2	0	2000	800
86	3.77	5.09	24	1500	100	23	2.75	6.81	0	2000	1300
87	2.68	5.18	24	1500	800	24	3.38	7.23	0	2000	1500
88	3.27	6.97	24	1500	1300	25	2.56	7.54	0	2000	1700
89	2.79	7.47	24	1500	1500	26	2.66	5.1	18	1300	100
90	3.02	7.98	24	1500	1700	27	2.46	5.16	18	1300	800
91	3.03	5.09	24	1900	100	28	2.54	6.6	18	1300	1300
92	2.45	5.17	24	1900	800	29	2.51	6.87	18	1300	1500
93	3.55	6.98	24	1900	1300	30	2.61	7.13	18	1300	1700
94	3.57	7.6	24	1900	1500	31	3.06	5.09	18	1400	100
95	3.44	8.21	24	1900	1700	32	3.23	5.18	18	1400	800
96	3.06	5.09	24	2000	100	33	2.85	6.76	18	1400	1300
97	2.57	5.17	24	2000	800	34	2.52	7.12	18	1400	1500
98	3.29	6.98	24	2000	1300	35	2.36	7.39	18	1500	1700
99	2.69	7.58	24	2000	1500	36	2.9	5.09	18	1500	100
100	2.3	8.21	24	2000	1700	37	2.94	5.2	18	1500	800
101	2.99	5.09	48	1300	100	38	2.44	6.84	18	1500	1300
102	3.37	6.98	48	1300	800	39	2.39	7.3	18	1500	1500
103	2.37	7.58	48	1300	1300	40	2.83	7.62	18	1500	1700
104	2.29	7.58	48	1300	1500	41	3.02	5.09	18	1900	100
105	2.5	8.18	48	1300	1700	42	2.48	5.17	18	1900	800
106	3.03	5.09	48	1400	100	43	2.82	7.01	18	1900	1300
107	4.1	5.17	48	1400	800	44	5.88	7.59	18	1900	1500
108	3.23	6.98	48	1400	1300	45	2.42	8.13	18	1900	1700
109	2.35	7.58	48	1400	1500	46	3.01	5.13	18	2000	100
110	5.55	8.18	48	1500	1700	47	3.34	5.17	18	2000	800
111	3.78	5.09	48	1500	100	48	2.35	6.99	18	2000	1300
112	2.42	5.17	48	1500	800	49	2.34	7.62	18	2000	1500

113	2.6	6.98	48	1500	1300	50	2.79	8.16	18	2000	1700
114	6.31	7.58	48	1500	1500	51	2.75	5.09	22	1300	100
115	2.29	8.18	48	1500	1700	52	2.98	5.18	22	1300	800
116	3.03	5.09	48	1900	100	53	2.8	6.76	22	1300	1300
117	2.43	5.17	48	1900	800	54	2.5	7.11	22	1300	1500
118	4.04	6.98	48	1900	1300	55	2.93	7.39	22	1300	1700
119	3.64	7.58	48	1900	1500	56	3.03	5.09	22	1400	100
120	3.83	8.18	48	1900	1700	57	3.06	5.2	22	1400	800
121	2.7	5.09	48	2000	100	58	2.36	6.85	22	1400	1300
122	3.11	5.17	48	2000	800	59	2.99	7.31	22	1400	1500
123	2.39	6.98	48	2000	1300	60	3.32	7.63	22	1500	1700
124	2.34	7.58	48	2000	1500	61	3.03	5.09	22	1500	100
125	2.34	8.18	48	2000	1700	62	3.02	5.18	22	1500	800
						63	3.23	6.93	22	1500	1300

In-situ testing:

The analysis of the settlement of the body of earth dams, in addition to calculating the amount of water loss, plays a fundamental role in calculating the amount of pore water and consequently in stability analysis. Furthermore, any settlement analysis is dependent on the hydraulic properties of the materials constituting the dam. To investigate the effect of hydraulic conductivity parameters on the settlement phenomenon, a laboratory model of an earth dam was constructed and examined by accurately measuring the hydraulic parameters of the materials in both saturated and unsaturated States



Figure 4: Excavation and control of the dam model within the ground and the completion of the earthen dam plaster.

Initially, to measure the required parameters and clarify the obstacles of the earth dam model in natural soil, a model was executed where necessary waterproofing was performed using a pressure brick wall along with cement plaster. Preliminary studies and modeling were conducted, but issues such as rainfall, changes in water level, and the inability to control the internal environment of the

device led to the decision to construct the device with glass and a metal frame.

The distribution of moisture in porous environments under the conditions of permanent and non-permanent seepage flows is of significant interest in many issues, including the theory of settlement from the foundation and body of the earth dam, the interaction of surface waters with groundwater, seepage and water loss from water transfer channels, various environmental issues, and studies on the spread and dispersion of pollution. Many researchers have focused on seepage flow in unconfined environments with a free surface, and recently new methods have been proposed for analyzing such issues. For example, non-permanent seepage flow affected by rainfall and water level fluctuations has been examined using the saturated-unsaturated seepage model based on the two-phase flow theory of water and air in porous media.

The proposed solution method known as the expanded pressure method solved the seepage problem with a free flow surface by employing a unit step function (Heaviside) of 0 and 1. In recent years, with modifications to the Heaviside function condition, the expanded pressure method has been efficiently refined, significantly improving the convergence of the seepage relationship solution in unconfined conditions. Many of the proposed models depend on water pressure or hydraulic load. As a result, in these numerical models and methods, due to the phenomenon of capillarity, it is not possible to accurately determine the contact surface between water and air. Additionally, due to the severe changes in soil saturation near this surface, accurately determining the position of the phreatic surface is challenging. Therefore, to accurately determine the position of the seepage surface and the phreatic line, it is necessary to specify the changes in hydraulic conductivity of the porous medium in the unsaturated state. In fact, the limitation of using seepage analysis models relates to determining the hydraulic properties of the medium, especially the changes in moisture and consequently the changes in permeability of the medium in unsaturated conditions. This research examined the impact of using unsaturated hydraulic properties of soil materials on the phenomenon of unconfined seepage from earth dam bodies. Accordingly, the position of the seepage line, water pressure distribution, and the amount of flow passing through the foundation of the homogeneous earth dam were studied.

Laboratory Model:

To investigate the phenomenon of seepage in the bodies of earth dams, a laboratory model of a homogeneous earth dam with a height of 31.75 centimeters was constructed symmetrically relative to the dam axis (the scale of the constructed device is 1:400). To examine the seepage line and pore water pressure in the dam body, numerous piezometers were used with a distance of 10 to 15 centimeters apart and arranged in several rows according to the dimensions. Given the height of the dam, the width of the toe was calculated to be 26.98. (The slope ratio of the dam is 1 to 1.5, and the width of the dam crest is 12 meters).

Considering that it is desirable for studies to be conducted 1.5 times the width of the toe, the foundation of the dam was assumed to be 147.39 centimeters on each side, thus the device was planned to be 4 meters long. The width of the device was assumed to be a unit, and since the depth of the waterproofing wall at its highest point was 78 meters, the height of the device needed to be more than 51.25 centimeters, which, accounting for one-meter bases, was considered to be 151.25 centimeters. However, to enhance the comprehensiveness of the device, a net height of 2 meters was considered in the construction.

The constructed device was made of glass framed to allow for peripheral examination. These frames were designed to be vertical, ensuring that the pressure on each glass frame was equal and

allowing for examination at different heights. Additionally, since the width of the frames was calculated to be about 90 centimeters, several holes were created on the glasses horizontally for the installation of piezometers, resulting in a distance between piezometers of less than 15 centimeters, while this distance was limited to the same 15 centimeters vertically (in three rows).

According to the designed device, piezometers were installed at all points of the dam sample body with a chessboard distance of 15 centimeters. This process, in addition to being used as a piezometer, allows for the calculation of the output flow from each of the openings, which is one of the strengths of the designed device.

The materials used in the laboratory modeling were exactly the same as those used in the Karkheh Dam, which included Bakhtiari conglomerate. Based on the grading curve and dimensional analysis, and using the results of soil mechanics tests conducted by the Iranian government in the central province, suitable and similar soil was identified and used as the foundation. Other specifications of the dam are assumed to be in accordance with the specifications of the Karkheh Dam, but since the subject of this thesis is the foundation of the dam and, of course, the changes in the waterproofing wall, the dam body was constructed as a homogeneous dam.



Figure 5: Simulated soil of the Karkheh dam (in terms of specifications)

In the base section of the model, a rough-surfaced plate was used to reduce leakage flow at the contact point between the soil and the model body. Additionally, to minimize leakage at the contact points of the model's side walls and the soil, a layer of fine sand with adhesive was applied to the surfaces of the side walls. This not only reduces leakage flow at this surface but also increases friction between the soil and the wall surface of the model, preventing the phenomenon of soil separation from the side plates of the model. The side plates of the model were made of plexiglass, while the other parts were made of steel. Water reservoirs with the capability to control water levels were considered at both the upstream and downstream sides of the dam to examine the conditions of transient settlement in the model.

Specifications of the physical model body and the testing process:

In every settlement phenomenon, in addition to the geometry and boundary conditions, the characteristics of the materials play a significant role in the form and flow pattern. For the physical model of the Karkheh dam, soil with a simulated grading similar to Bakhtiari conglomerate containing a small percentage of silt was used. The body of the dam was constructed using a mixture with the grading of the dam. The reason for using such materials is their quick response to changes in boundary conditions, which in turn saves time. For constructing the dam body, layers of soil were poured with a thickness of 5 centimeters and compacted using a manual roller. Permeability measurement tests were conducted after the settlement tests were completed.

Since in the stability analysis and design of earth dams, non-permanent analysis is generally performed for the sudden drop in water level, non-permanent leakage tests were also conducted for this condition. The amount of leakage passing through the dam body at the outlet of the

laboratory model was measured in weight. Considering that the main objective of this research is to study the impact of hydraulic parameters of the dam body and foundation materials with changes in the specifications of the water-stop wall in the analysis of leakage from the earth dam body (Karkheh), multiple piezometers were used to determine the pore water pressure throughout the foundation and body of the dam.

Governing Equations

The volumetric moisture content is dependent on changes in stress state and the physical properties of the soil. This equation is usually solved using one of the numerical methods of finite elements or finite differences.

Since the aim of this research was to investigate the impact of transfer functions including hydraulic conductivity and the moisture characteristic curve in the numerical modeling of the seepage problem in the Karkheh earth dam, and considering the various types of flow in steady and unsteady states, the results were examined based on different conditions and presented according to the combination of various conditions and functions.

Given that the body of the earth dam was constructed in 5-centimeter layers, anisotropy in the hydraulic conductivity parameter of the body was a given. To determine the ratio of horizontal to vertical hydraulic conductivity, based on the data obtained from seepage tests from the body and foundation of the dam at the maximum water level (18 centimeters) in both steady and unsteady conditions, the model was calibrated based on the anisotropy of the hydraulic conductivity of the body. The reason for choosing this level was to accurately simulate the Karkheh dam .



Figure 6: Transparent chamber of the earth dam model and the waterproof wall mold

Waterproof wall:

The mold prepared is exactly equivalent to the width of the device and a height of 19.5 centimeters and a thickness of one centimeter. To repair the waterproof wall, rabbit sheets were used.

The mix design of the plastic concrete for the waterproof wall includes a combination of water, cement, aggregate materials, and bentonite, prepared according to the mix design of previous tests (determining compressive strength) as per the table below and poured into the molds.

Table 4: Specifications of the mixing design of waterproof wall samples

Bentonite (warm)	Bentonite (warm)	adhesive materials (hot)	sample number
163.25	29.25	292.5	1
307.125	34.125	341.25	2
351	39	390	3
234	58.5	292.5	4
273	68.25	341.25	5
312	78	390	6
204.75	87.75	292.5	7
238.875	102.375	341.25	8

273	117	390	9
175.5	117	292.5	10
204.75	136.5	341.25	11
234	156	390	12
146.25	146.25	292.5	13
170.625	170.625	341.25	14
195	195	390	15
117	175.5	292.5	16
136.5	204.75	341.25	17
156	234	390	18

After the final setting of the plastic concrete, the waterproof wall panels were placed in their position, and then the body of the dam was constructed, followed by the filling of the testing device.



Figure 7: Placing the waterproof wall under the dam model

Test Results:

In this series of experiments, the impermeable walls were prepared according to the mixing design mentioned above, and two parameters, the pore water pressure in the body and foundation of the dam, as well as the outflow rate, were studied.

The amount of leakage water from the dam (water transferred from upstream to downstream) was measured at the end of each day, and for example, regarding impermeable wall number one, the leakage is as shown in the graph below.

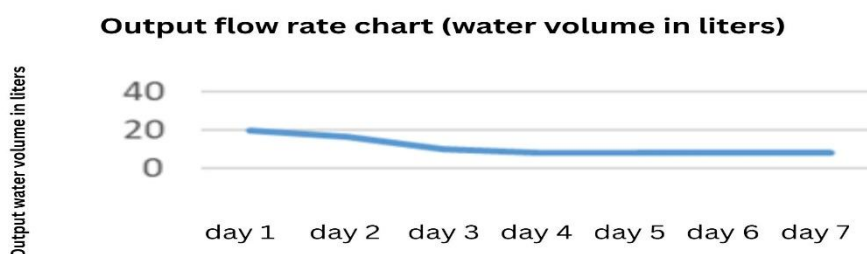


Figure 8: Output flow rate chart

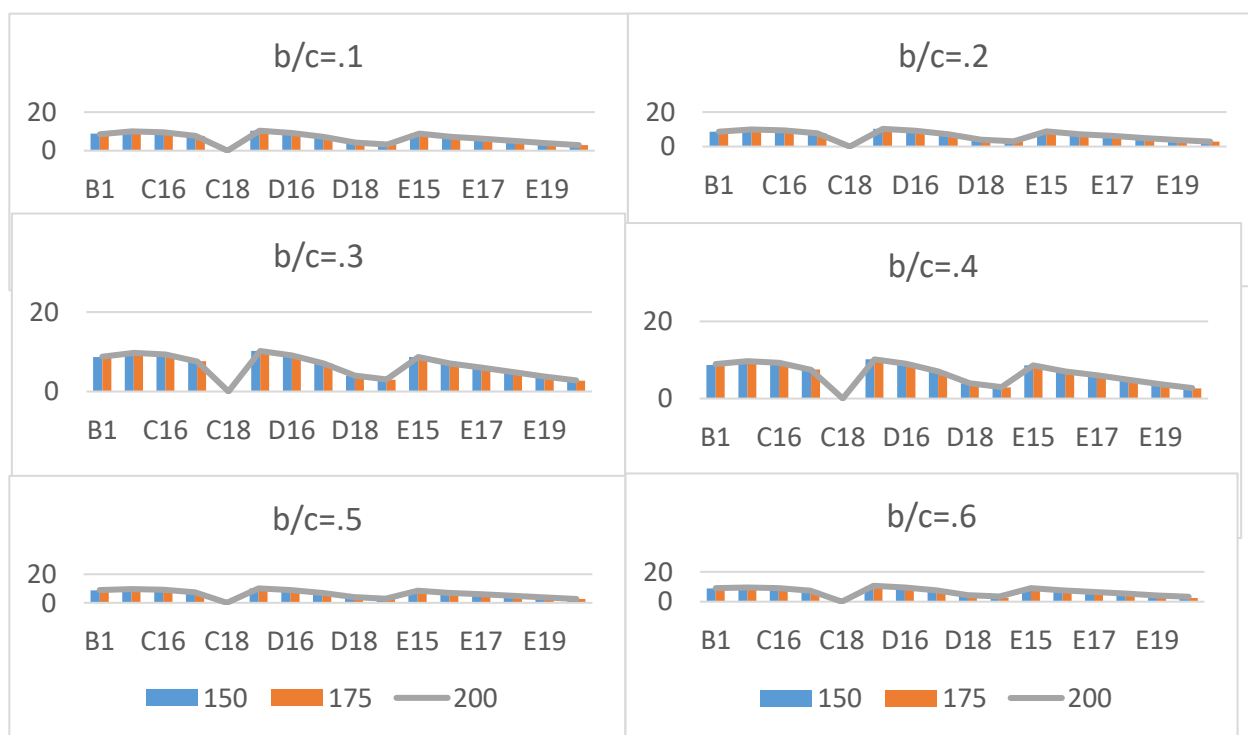
The graph indicates that the high seepage occurred during the initial days of filling, and from the fourth day onwards, the output flow rate remained constant at 8 liters. The output flow rate for 18 samples is approximately equal, and since examining this topic is not the focus of this thesis, we will refrain from studying it.

Pore Water Pressure:

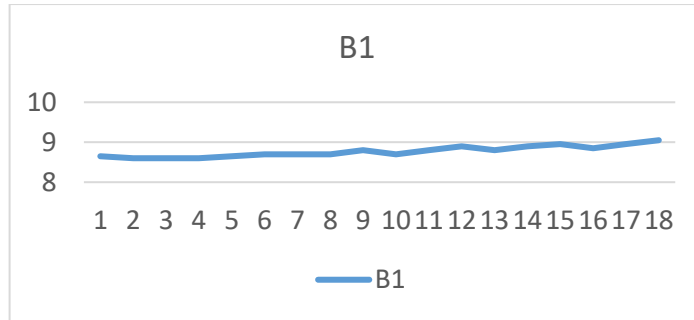
The pore water pressure was examined at each of the piezometers installed in the body and foundation of the dam, and the results are as shown in the table below (the piezometers are labeled in 5 rows from A to E from top to bottom, and the rows are numbered from left (upstream) to right (downstream)).

Results Analysis:

The pore water pressure was calculated for 18 samples, which are displayed in 6 graphs with a bentonite-to-cement ratio ranging from 0.1 to 0.6. Each graph contains three diagrams (for concrete grades 150, 175, and 200). These 18 samples correspond to 20 piezometers in the middle of the device. In piezometers c19, c20, and d20, the desired pressure was not present, so they were excluded from the study ..



As shown in the above charts, we are facing a pressure drop in every row and also in the rows. Here, it is necessary to conduct an investigation by changing the waterproofing walls and for each of the piezometers.



.Figure 10: Graph of pressure changes in piezometer B1 with changes in the waterproofing walls

In the piezometer graph B1, the charts for samples 1, 2, and 3 are almost horizontal, and no significant changes are observed. However, the overall trend of the graph is upward. In this context, a drop is observed with the change in the ratio of bentonite to cement, which is due to the reduction in the amount of cement used.

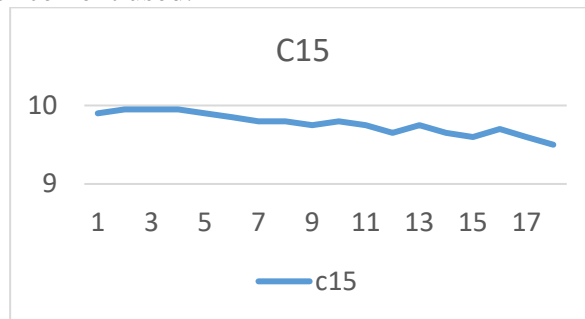


Figure 11: Pressure variation chart in piezometer C15 with changes in the waterproofing walls

In piezometer number C15, the graphs for samples 1, 2, and 3 are almost horizontal, showing no significant changes; however, the overall trend of the graph is downward. In this context, a drop is observed with the change in the ratio of bentonite to cement, which is due to the reduction in the amount of cement used.

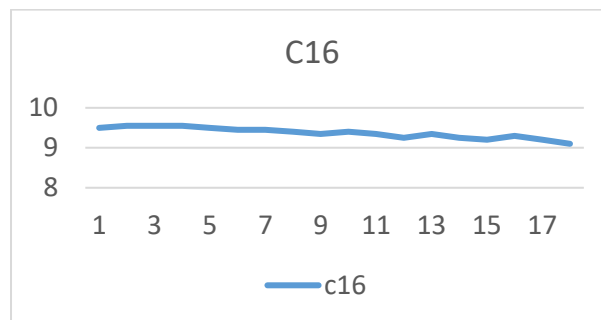


Figure 12: Graph of pressure changes in piezometer C16 with changes in the waterproofing walls

In piezometer number C16, the graphs for samples 1, 2, and 3 are almost horizontal, and no significant changes are observed. However, the general trend of the graph is downward. In this context, a drop is observed with the change in the ratio of bentonite to cement, which is due to the reduction in the amount of cement Use

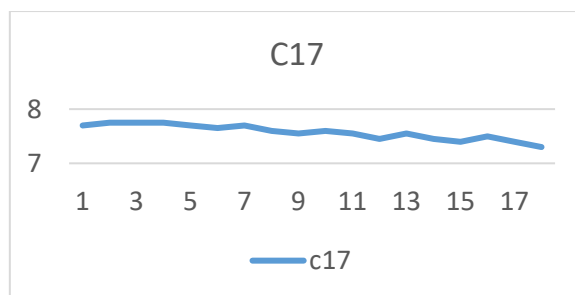


Figure 13: Graph of pressure changes in piezometer C17 with changes in the waterproofing walls

In piezometer number C17, the graphs for samples 1, 2, and 3 are almost horizontal, and no significant changes are observed. However, the general trend of the graph is downward. In this context, a drop is observed with the change in the ratio of bentonite to cement, which is due to the reduction in the amount of cement used.

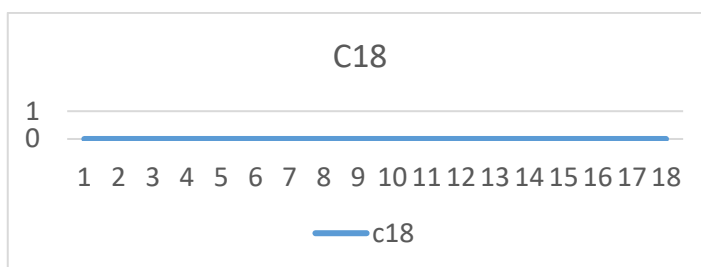


Figure 14: Pressure variation chart in piezometer C18 with changes in the cutoff walls

In piezometer number C18, considering that this piezometer is located directly beneath the dam body and behind the cutoff wall, the flow pipes do not reach this area, and the pressure in this piezometer has become zero ..

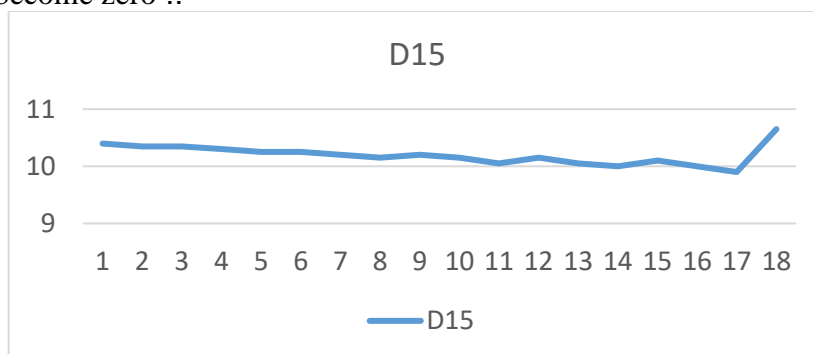


Figure 15: Diagram of pressure changes in piezometer D15 with changes in the waterproofing walls.

In piezometer D15, we are facing a relatively stable descending trend, and in this piezometer, in the last sample which has the lowest amount of cement, despite the trend of the graph, there has been a pressure spike in the piezometer.

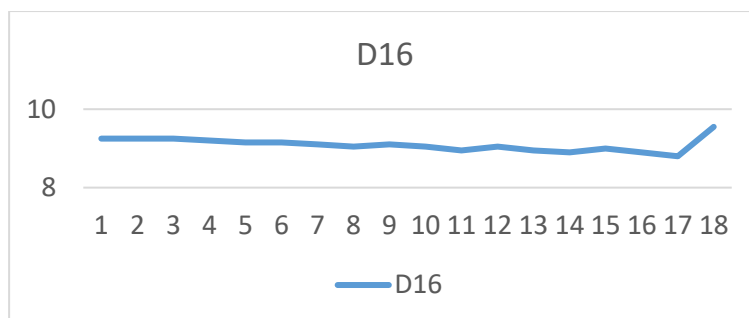


Figure 16: Pressure variation chart in piezometer D16 with changes in the waterproofing walls

In piezometer D16, we are facing a relatively stable descending trend, and in this piezometer, in the last sample which has the lowest amount of cement, despite the trend of the chart, there has been a pressure spike in the piezometer.

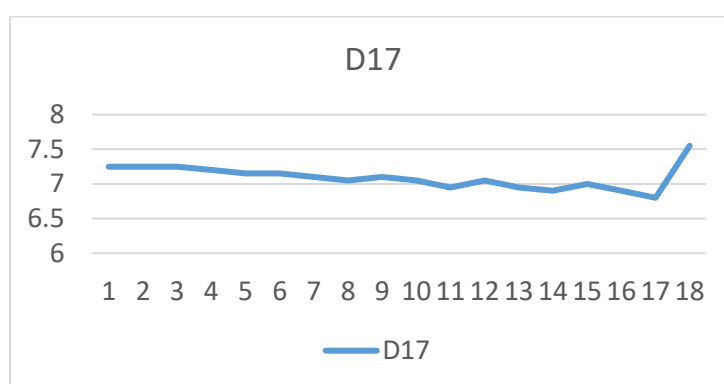


Figure 17: Chart of pressure changes in piezometer D17 with changes in the waterproofing walls

In piezometer D17, we are facing a relatively stable downward trend, and in this piezometer, in the last sample which has the lowest amount of cement, despite the trend of the chart, there has been a pressure spike in the piezometer.

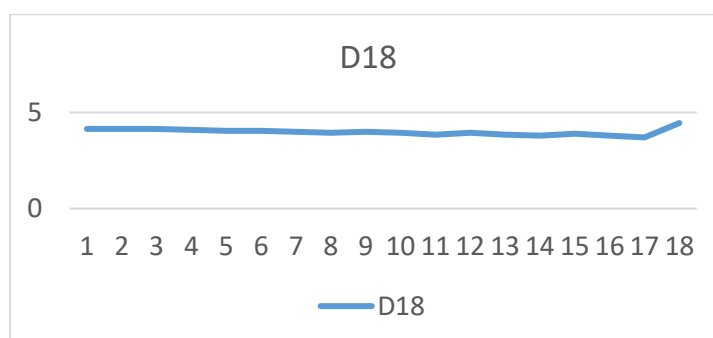


Figure 18: Pressure variation chart in piezometer D18 with changes in the impermeable walls

In piezometer D18, although we are facing a downward trend, the difference between the maximum and minimum is so small that the changes are not noticeable. In this piezometer, in the last sample which has the least amount of cement, despite the trend of the chart, there has been a pressure spike in the piezometer.

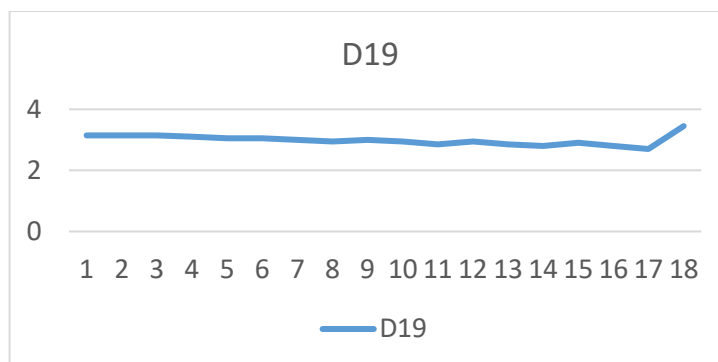


Figure 19: Pressure variation chart in piezometer D19 with changes in the impermeable walls

In piezometer D19, although we are facing a downward trend, the difference between the maximum and minimum is so small that the changes are not noticeable. In this piezometer, in the last sample which has the least amount of cement, despite the trend of the chart, there has been a pressure spike in the piezometer.

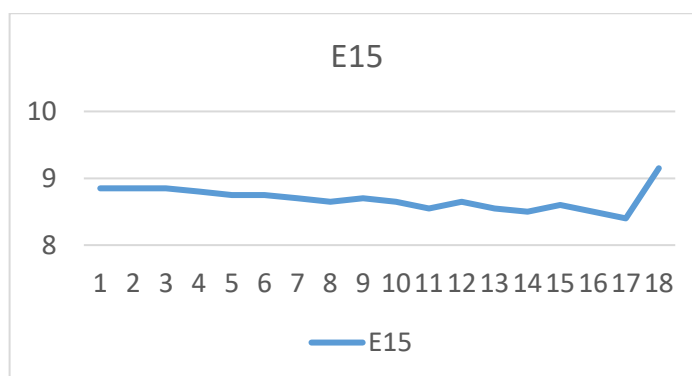


Figure 20: Chart of pressure changes in piezometer E15 with changes in the waterproofing walls

In piezometer E15, we are facing a relatively stable downward trend, and in this piezometer, in the last sample which has the lowest amount of cement, despite the trend of the chart, there has been a pressure spike in the piezometer.

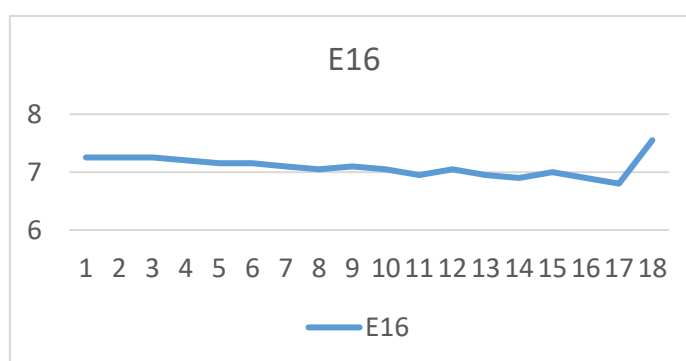


Figure 21: Pressure variation chart in piezometer E16 with changes in the impermeable walls

In piezometer E16, we are facing a relatively stable downward trend, and in this piezometer, in the last sample which has the lowest amount of cement, despite the trend of the chart, there has been a pressure spike in the piezometer ..

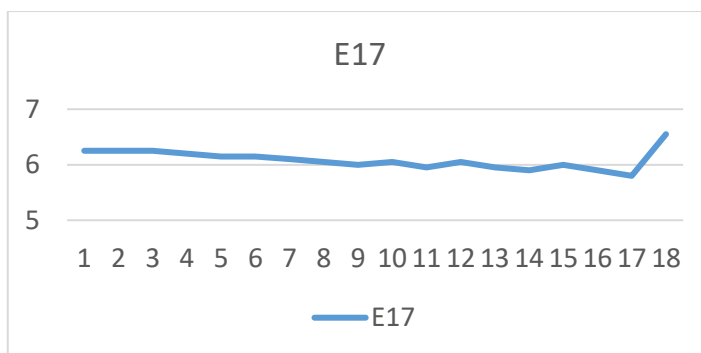


Figure 22: Pressure variation chart in piezometer E17 with changes in the impermeable walls

In piezometer E17, we are faced with a relatively stable downward trend, and in this piezometer, in the last sample which has the lowest amount of cement, despite the trend of the chart, there has been a pressure spike in the piezometer.

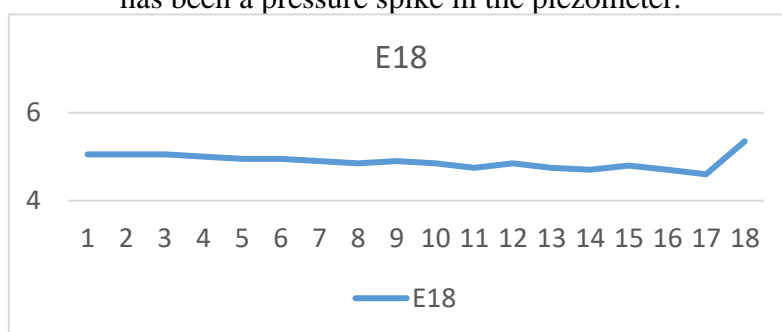


Figure 23: Pressure variation chart in piezometer E18 with changes in the waterproofing walls

In piezometer E18, we are facing a relatively stable downward trend, and in this piezometer, in the last sample which has the lowest amount of cement, despite the trend of the chart, there has been a pressure spike in the piezometer.

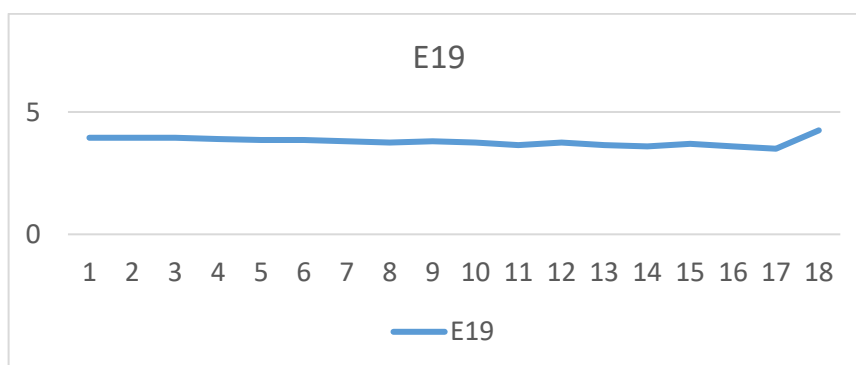
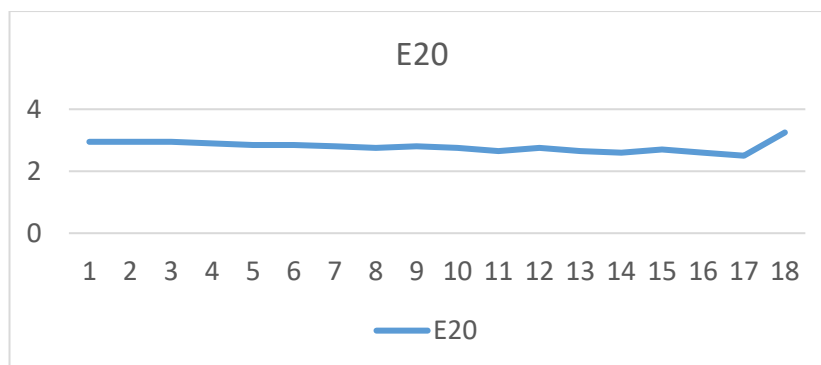


Figure 24: Pressure variation chart in piezometer E19 with changes in the impermeable walls

In piezometer E19, although we are facing a downward trend, the difference between the maximum and minimum is so small that the changes are not noticeable. In this piezometer, in the last sample which has the least amount of cement, despite the trend of the chart, there has been a pressure spike in the piezometer.



25. The graph of pressure changes in piezometer E20 with changes in the impermeable walls

In piezometer E20, although we are facing a downward trend, the difference between the maximum and minimum is so small that the changes are not noticeable. In this piezometer, in the last sample which has the least amount of cement, despite the trend of the graph, there has been a pressure spike in the piezometer .

Conclusion

In this research, the phenomenon of seepage from the foundation of the Karkheh earth dam was investigated using the Plaxis computational code, studying the effects of parameters influencing this phenomenon. The results indicate that the flexibility of the cutoff wall was examined based on the maximum displacement of the cutoff wall without any failure occurring in it, and an optimal combination of materials for one cubic meter of concrete was proposed. Overall, the results indicate that sample number 18 is not scientifically acceptable, while other technical specifications and results demonstrate the impact of cement content, both in terms of grades (150, 175, and 200) and in terms of the ratio of bentonite to cement from 0.1 to 0.6, showing a direct relationship between the amount of cement and the pore water pressure across the entire dam sample and the permeability of the cutoff wall.

References:

1. Rahimi, H. (1389), "Embankment Dams," University of Tehran press, Iran, 671pp.
2. Hu, L., Wu, X., Liu, Y., Meegoda, J.N., Gao, S., 2010. Physical modeling of air flow during air sparging remediation. *Environ. Sci. Technol.* 44 (10), 3883–3888.
3. Du, Y.J., Jiang, N.J., Liu, S.Y., Jin, F., Singh, D.N., Puppala, A.J., 2014a. Engineering properties and microstructural characteristics of cement-stabilized zinc-contaminated kaolin. *Can. Geotech. J.* 51 (3), 289–302.
4. Du, Y.J., Wei, M.L., Reddy, K.R., Liu, Z.P., Jin, F., 2014b. Effect of acid rain pH on leaching behavior of cement stabilized lead-contaminated soil. *J. Hazard. Mater.* 271, 131– 40.
5. Xue, Q., Li, J.S., Liu, L., 2013. Experimental study on anti-seepage grout made of leachate contaminated clay in landfill. *Appl. Clay Sci.* 80–81, 438–442.
6. Evans, J.C., Costa, M.J., Cooley, B., 1995. The state-of-stress in soil–bentonite slurry trench cutoff walls. In: Acar, Y.N., Daniel, D.E. (Eds.), *Geoenvironment 2000: Characterization, Containment, Remediation, and Performance in Environmental Geotechnics*. ASCE GSP 46. ASCE, Reston, VA, pp. 1173–1191.
7. Sharma, H.D., Reddy, K.R., 2004. *Geoenvironmental Engineering: Site Remediation, Waste Containment, and Emerging Waste Management Technologies*. John Wiley and Sons Inc., New York.
8. Malusis, M.A., Barben, E.J., Evans, J.C., 2009. Hydraulic conductivity and compressibility of soil–bentonite backfill amended with activated carbon. *J. Geotech. Geoenviron. Eng.* ASCE 135 (5), 664–672.

9. Ruffing, D.G., Evans, J.C., Malusis, M.A., 2010. Prediction of earth pressures in soil– bentonite cutoff walls. In: Fratta, D.O., Puppala, A.J., Muhunthan, B. (Eds.), *GeoFlorida 2010: Advances in Analysis, Modeling and Design*. ASCE GSP 199. ASCE, Reston, VA, pp. 2416–2425.
10. Hong, C.S., Shackelford, C.D., Malusis, M.A., 2010. Consolidation and hydraulic conductivity of zeolite amended soil–bentonite backfills. *J. Geotech. Geoenviron. Eng. ASCE* 138 (1), 15–25.
11. Fan, R.D., Du, Y.J., Reddy, K.R., Liu, S.Y., Yang, Y.L., 2014a. Compressibility and hydraulic conductivity of clayey soil mixed with calcium bentonite for slurry wall backfill: initial assessment. *Appl. Clay Sci.* 101, 119–127.
12. Malusis, M.A., McKeehan, M.D., 2013. Chemical compatibility of model soil–bentonite backfill containing multiswellable bentonite. *J. Geotech. Geoenviron. Eng. ASCE* 139 (2), 189–198.
13. Yong, R.N., Ouhadi, V.R., Goodarzi, A.R., 2009. Effect of Cu²⁺ ions and buffering capacity on smectite microstructure and performance. *J. Geotech. Geoenviron. Eng. ASCE* 135 (12), 1981–1985.